Test of the Universal Scaling Law of Diffusion in Colloidal Monolayers

Xiaoguang Ma,[1] Wei Chen,[2] Ziren Wang,[1] Yuan Peng,[1] Yilong Han,[1] and Penger Tong[1,*]

[1]*Department of Physics, Hong Kong University of Science and Technology, Clear Water Bay, Kowloon, Hong Kong*
[2]*State Key Laboratory of Surface Physics and Department of Physics, Fudan University, Shanghai 200433, China*

Using the techniques of optical microscopy and particle tracking, we measure the pair correlation function and Brownian diffusion in monolayers of strongly interacting colloidal particles suspended at or near three different interfaces and test the universal scaling law of the normalized diffusion coefficient, $\tilde{D} \simeq e^{\alpha \Delta S}$, as a function of the excess entropy ΔS for a wide range of particle concentrations. It is found that the universal scaling law with $\alpha = 1$ holds well for highly charged polystyrene spheres suspended at an air-water interface, where the strong electrostatic interactions play a dominant role. For monolayer suspensions of hard-sphere-like particles, where hydrodynamic interactions become important, deviations from the universal scaling law are observed. The experiment indicates that the hydrodynamic corrections could be incorporated into the universal scaling law of diffusion with an exponent $\alpha < 1$.

Introduction.—Finding a relationship between structural properties and transport coefficients in liquids and glassy systems is an interesting but challenging problem in condensed matter physics [1]. Such a relationship is of fundamental importance because it affects our understanding of a wide variety of disordered materials, including dense fluids, liquid metals and alloys, polymer solutions and melts, colloids, and grains [2]. With increasing concentration or decreasing temperature, the number of accessible microstates (or "free volume") to the particles in the solution is reduced and, thus, the motion of the particles is hindered, resulting in a slowing down of dynamics in the liquids and glassy systems. In 1996, Dzugutov [3] proposed a universal scaling law for dense liquids, which connects the normalized diffusion coefficient $\tilde{D}$ with the excess entropy ΔS per molecule relative to an ideal gas, $\tilde{D} = Ae^{\Delta S}$, where A is a numerical constant and ΔS is expressed in units of Boltzmann's constant k_B. This equation provides an intriguing example of structure-dynamics relations, which connects a dynamic quantity ($\tilde{D}$) to a structural one (ΔS).

The proposed scaling law has stimulated considerable numerical efforts aimed at testing it in simple fluids [4,5], binary fluid mixtures [6,7], and liquid metals [8,9]. In contrast to the large number of numerical studies, experimental investigations of the universal scaling law are rare. This is partially due to the fact that it is quite difficult to obtain both the diffusion and pair correlation data in simple liquids or in liquid metals.

In this Letter, we report a systematic investigation of the scaling law via simultaneous measurements of the diffusion coefficient and pair correlation function in monolayer suspensions of strongly interacting colloidal particles. The colloidal monolayers offer many advantages over atomic or molecular fluids, because the dynamics of the particles are slower and can be tracked at the single-particle level

with video microscopy [10]. They have served as a model system to study a range of interesting problems in two-dimensional (2D) soft matter physics [11]. Examples include 2D crystallization [12,13] and grain-boundary fluctuations [14], crystal sublimation [15] and colloidal glasses [16,17], interactions between similarly charged particles [18–21], and Brownian dynamics at liquid interfaces [22–25]. Since the colloidal systems are 2D and clearly visible, precise measurements of particle configurations and motion can be carried out conveniently. Moreover, our experiment explores both the long-ranged and short-ranged thermodynamic interactions, whereas the numerical simulations only focused on idealized, short-ranged atomic potentials, such as Lennard-Jones potentials, with relatively small numbers of particles and molecular configurations [3,5,26].

Experimental methods.—Three kinds of colloids are used in the experiment, and their properties are given in Table I. The first two are polystyrene (PS) latex spheres; PS1 has carboxyl groups and PS2 has sulfate groups on their surfaces. The third is silica spheres, which have SiO^- groups on the surface. The three types of colloidal spheres are all negatively charged. In the experiment, we disperse PS1 and PS2 at an air-water interface following the same procedures as described in Ref. [21]. With the known surface tensions, it was estimated that 2/3 of the PS particle (by diameter) is immersed in water and 1/3 is in air. The silica spheres are dispersed near two different interfaces. $SiO_2 1$ and $SiO_2 2$ are sandwiched between two glass slides, and they settle down near the bottom water-glass interface by gravity. The spacing between the two glass slides is 0.5 mm, which is much larger than the particle diameter d (2–3 μm) and the gap distance (0.2–0.7 μm) between the particle surface and the substrate due to thermal fluctuations and electrostatic repulsions.

TABLE I. Colloidal samples used in the experiment. The particle diameter d and surface charge density σ are provided by the manufactures.

Sample	$d(\mu m)$	$\sigma(\mu C/cm^2)$	d^*/d	Interface
PS1	1.1 ± 0.02	-12.5	11.7	Air-water
PS2	1.0 ± 0.03	-2.8	6.9	Air-water
$SiO_2 1$	3.01 ± 0.03	-0.01	1.1	Water-glass
$SiO_2 2$	2.14 ± 0.02	-0.01	1.2	Water-glass
$SiO_2 3$	2.14 ± 0.02	-0.01	1.1	Water-air

$SiO_2 3$ is filled into a cylindrical cell of 2 mm in height and 6 mm in diameter with its top sealed by a cover slip and bottom kept open. The capillary force is large enough to keep the solution suspended against gravity, and a water-air interface is formed with the water on top of the air [27]. By adjusting the volume of the solution inside the cell, the water-air interface can be kept flat. From direct observation of a particle's real-time motion, we find that the $SiO_2 3$ spheres settle down toward the bottom water-air interface, but their surface has not yet intersected with the liquid interface. More experimental details are given in the Supplemental Material [28].

The sample cell is viewed under an inverted microscope, and the motion of the interfacial particles is recorded with a digital camera. A particle tracking program is used to determine the particle position $\mathbf{r}(t)$ at time t, and the particle trajectories are constructed from the consecutive images. From the particle trajectories, we obtain the single-particle mean square displacement, $\langle \Delta \mathbf{r}^2(\tau) \rangle = \langle |\mathbf{r}(t+\tau) - \mathbf{r}(t)|^2 \rangle$, as a function of delay time τ. Using the same image data, we calculate the pair correlation function $g(r)$ [21] and the two-body excess entropy S_2 per particle [29],

$$S_2 = -\frac{4n}{d^2} \int_0^\infty \{g(r) \ln[g(r)] - [g(r) - 1]\} r dr, \quad (1)$$

where n is the area fraction occupied by the interfacial particles. In the original work of Dzugutov [3], S_2 was used to approximate the total excess entropy $\Delta S \simeq S_2$. It was shown that S_2 contributes $\sim 90\%$ of ΔS for the Lennard-Jones system over a wide range of densities [29].

Results and discussion.—Figure 1 compares the measured $g(r)$ of five different colloidal samples at the small n limit. In the plot, the interparticle distance r is scaled by d. All the PS spheres show a long-range soft-core repulsion with $g(r)$ rising gradually with increasing r/d. The interaction range increases with the surface charge density σ. PS1 has the largest σ and longest repulsive range. The measured $g(r)$'s for the PS samples with different σ show a similar shape. It has been shown [21] that the interaction potential $U(r)$ for the PS spheres can be well described by a $1/r^3$ repulsion, resulting from the interaction between the induced out-of-plane dipoles at the interface. By contrast, the measured $g(r)$ for the silica samples displays a sharp rise at $r/d \simeq 1$, suggesting that the interaction between the
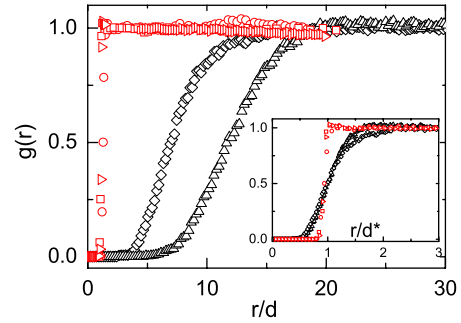
FIG. 1 (color online). Comparison of the measured $g(r)$ as a function of r/d for five colloidal samples: PS1 (black up-triangles), PS2 (black diamonds), $SiO_2 1$ (red squares), $SiO_2 2$ (red circles), and $SiO_2 3$ (red right-triangles). The measurements are made at the area fractions $n = 1.6 \times 10^{-3}$ for PS1 and PS2 and $n \simeq 0.01$ for $SiO_2 1$, $SiO_2 2$, and $SiO_2 3$. Inset shows $g(r)$ as a function of the normalized variable r/d^*.

silica spheres is short ranged and can be described by a hard-sphere-like potential [30].

To further quantify the interaction range, we replot $g(r)$ using a new variable r/d^* (inset of Fig. 1). Here we choose d^* so that $g(r) = 0.5$ at $r/d^* = 1$. Once r is scaled by the "effective hard-sphere diameter" d^*, the measured $g(r)$'s for the PS and silica samples collapse, respectively, onto two different master curves, indicating that the nature of the repulsion for the two types of colloids remains different. The obtained values of d^* for different samples are given in Table I with PS1 having the largest $d^* = 11.7d$, which is 10.6 times larger than that for $SiO_2 1$.

Figures 2(a) and 2(b) show, respectively, how the measured $g(r)$ for PS1 and $SiO_2 1$ changes with the area fraction n. Because of the strong long-ranged repulsion, $g(r)$ for PS1 begins to oscillate at a much smaller $n \simeq 3.8 \times 10^{-3}$, whereas for the weakly charged $SiO_2 1$, $g(r)$ begins to oscillate at $n \simeq 0.1$. Figure 2(a) reveals an important feature of the strongly charged colloidal system, namely, the development of a well-defined interparticle separation r_0 corresponding to the first dominant peak in $g(r)$. As n increases, r_0 decreases and the spatial confinement by the surrounding particles becomes more pronounced. We have verified that r_0 is proportional to the interparticle distance $l \approx d[\pi/(4n)]^{1/2}$. In fact, one can directly observe this characteristic length from the equilibrium particle configurations, as shown in the inset of Fig. 2(a). By contrast, the first dominant peak of $g(r)$ for the silica spheres remains unchanged, which is a feature of hard-sphere-like interactions. The inset of Fig. 2(b) shows an equilibrium particle configuration of $SiO_2 1$.

Figure 3 shows a log-log plot of the measured $\langle \Delta r^2(\tau) \rangle$ as a function of delay time τ for $SiO_2 2$ at two different area fractions. At small $n = 0.01$, $\langle \Delta r^2(\tau) \rangle$ is a linear function of τ over the entire range, which is a straight line in the log-log plot with a slope of unity (upper solid line), indicating that the particles are undergoing free diffusion. At large $n > 0.5$,
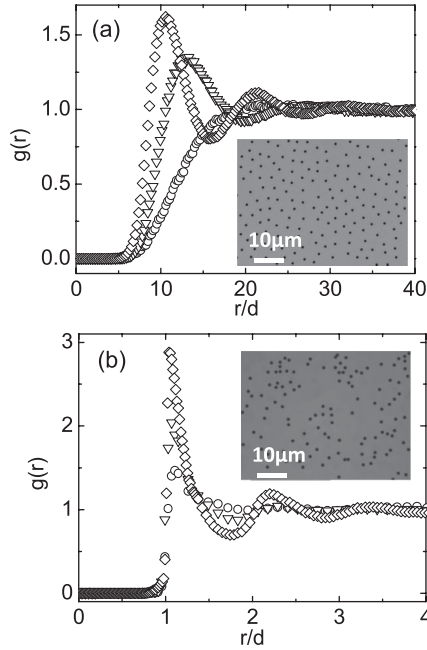
FIG. 2. (a) Measured $g(r)$ as a function of r/d for PS1 at $n = 1.6 \times 10^{-3}$ (circles), 3.8×10^{-3} (triangles), and 6.0×10^{-3} (diamonds). Inset shows the equilibrium configuration of PS1 at $n = 2.4 \times 10^{-2}$. (b) Measured $g(r)$ for $SiO_2 1$ at $n = 0.17$ (circles), 0.34 (triangles), and 0.52 (diamonds). Inset shows an equilibrium configuration of $SiO_2 1$ at $n = 4.1 \times 10^{-2}$.

however, $\langle \Delta r^2(\tau) \rangle$ curves down in the linear plot, showing a "cage hindering" to a particle due to the repulsion from the neighboring particles. In colloidal self-diffusion, one considers the motion of a tagged particle in the suspension. For short time intervals, the particle diffuses within the cage, giving rise to a short-time self-diffusion. For large time intervals, the particle can hop among different cages, giving rise to a long-time self-diffusion [1]. The lower solid and (red) dashed lines in Fig. 3 show, respectively, the long- and short-time self-diffusion of $SiO_2 2$. From the intercept of the
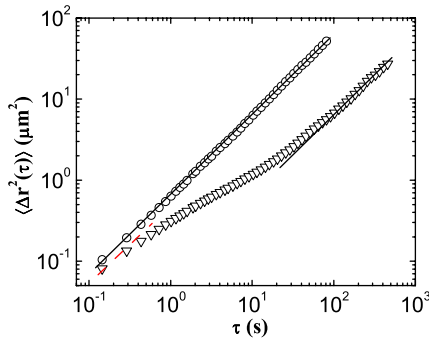
FIG. 3 (color online). Log-log plot of the measured $\langle \Delta r^2(\tau) \rangle$ as a function of τ for $SiO_2 2$ at $n = 0.01$ (circles) and 0.71 (triangles). The solid lines show the power-law fits of slope 1 to the data points at large τ and the (red) dashed line is the fit of slope 1 to the data points at small τ.

lower solid line, we obtain the long-time self-diffusion coefficient D_S^L. A similar effect is also observed for other PS and silica samples. Because of the strong repulsion, the hindering effect for the PS samples begins at a much smaller $n > 5 \times 10^{-3}$ compared with the silica samples.

Figure 4 shows how the measured D_S^L changes with n for the five colloidal samples. In the plot, D_S^L is scaled by the diffusion coefficient D_0 obtained at the low n limit for each sample. The behavior of D_0 for different colloid-interface systems has been carefully studied in recent experiments [22–25,30]. All the measured D_S^L/D_0 follow the same trend, that it decreases with n. The measured D_S^L/D_0 for the PS samples decays significantly faster than that for the silica samples. The inset shows a magnified plot indicating the difference between PS1 and PS2. The measured D_S^L/D_0 for the silica samples also shows different dependence on n with D_S^L/D_0 for $SiO_2 1$ decaying the fastest.

Figure 5 is a replot of D_S^L/D_0 as a function of $-S_2$. Using Eq. (1) and the measured $g(r)$, we calculate S_2 at various area fractions for each sample. While as a function of n they have different functional forms, the measured D_S^L/D_0's for different colloidal samples can all be well described by a simple scaling law,

$$\tilde{D} \equiv D_S^L/D_0 = e^{\alpha S_2}, \qquad (2)$$

where the value of α varies among the colloidal samples. All the PS samples at the air-water interface (PS1 and PS2) collapse onto a single master curve with $\alpha = 1$ (lower solid line). This result agrees with the universal scaling law originally proposed by Dzugutov [3] for simple liquids. The data from the silica samples near the glass wall ($SiO_2 1$ and $SiO_2 2$) can be described by Eq. (2) with $\alpha = 0.7$ (middle dashed line), and those for $SiO_2 3$ (near the water-air interface) can be described with $\alpha = 0.5$ (upper dashed line).

Previous simulation tests of the universal scaling law have considered the effect of direct thermodynamic interactions on dense fluids [4,5,8,9]. For the PS spheres at the air-water interface, their electrostatic interactions are long
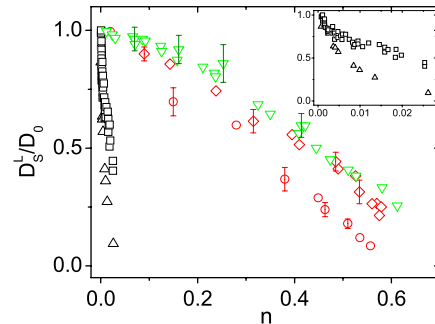
FIG. 4 (color online). Measured D_S^L/D_0 as a function of n for PS1 (black up triangles), PS2 (black squares), $SiO_2 1$ (red circles), $SiO_2 2$ (red diamonds), and $SiO_2 3$ (green down triangles). Inset shows a magnified plot for PS1 and PS2.
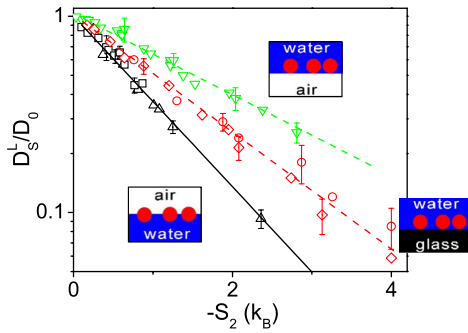
FIG. 5 (color online).   Measured D_S^L/D_0 as a function of $-S_2$ for PS1 (black up triangles), PS2 (black squares), $SiO_2 1$ (red circles), $SiO_2 2$ (red diamonds), and $SiO_2 3$ (green down triangles). The solid and dashed lines show the fits to Eq. (2) with $\alpha = 1$ (lower solid line), $\alpha = 0.7$ (middle dashed line), and $\alpha = 0.5$ (upper dashed line). The legends depict the three different interfacial systems under study.

ranged (unscreened) and play a dominant role in hindering the colloidal diffusion at the interface. Figure 5 thus demonstrates that for the colloidal samples (PS1 and PS2), in which the direct thermodynamic interactions are dominant, the universal scaling law as defined in Eq. (2) with $\alpha = 1$ works. In fact, the new variable, $S_2 \simeq \Delta S \sim \ln[\Omega(n, p)/\Omega_0]$, can be thought of as an entropy of distinct and thermally accessible colloidal configurations $\Omega(n, p)$ relative to those of an ideal gas Ω_0 [31]. Here $\Omega(n, p)$ is a function of both n and pressure p. For colloidal systems having the same n but with different interaction potentials, their pressure p is different. Figure 5, therefore, represents a comparison of the measured D_S^L/D_0 for different colloidal samples against a normalized configurational entropy, and Eq. (2) seems to indicate that $D_S^L/D_0 \simeq \Omega(n, p)/\Omega_0$, when $\alpha = 1$.

There are additional hydrodynamic interactions (HIs) between the colloidal particles, which are mediated through the solvent and affect the colloidal diffusion [1]. For the silica samples, because their direct thermodynamic interactions (TIs) are short ranged (hard-sphere-like), the HIs begin to play an increasingly important role at higher area fractions, where the near-field HIs (lubrication) become more pronounced [32]. In this case, the plot of D_S^L/D_0 vs n, as shown in Fig. 4, contains a mixed information of both the TIs and HIs. Figure 5 indicates that the combined hindering effect of the TIs and HIs can be described by the exponent α in Eq. (2). For $SiO_2 3$ the many-body HIs are long ranged (the single-body effect has been divided out by D_0) and the slip boundary condition at the liquid interface imposes a less hindering effect on D_S^L/D_0 ($\alpha = 0.5$). For $SiO_2 1$ and $SiO_2 2$, which are dispersed near a glass substrate, the nonslip boundary condition truncates the range of HIs and imposes a stronger hindering effect on D_S^L/D_0 ($\alpha = 0.7$). As mentioned above, the strong electrostatic repulsion between the PS

spheres gives rise to the strongest hindering effect ($\alpha = 1$). Clearly, a detailed modeling of HIs near the interface is needed in order to calculate α.

In summary, our experiment demonstrates that the universal scaling law as defined in Eq. (2) with $\alpha = 1$ holds well for highly charged PS spheres at an air-water interface, where the unscreened electrostatic interactions play a dominant role. Deviations from the universal scaling law are observed for monolayer suspensions of hard-sphere-like particles, where hydrodynamic interactions become important. The experiment indicates that the hydrodynamic corrections could be incorporated into the universal scaling law with $\alpha < 1$.

*penger@ust.hk

[1] P. N. Pusey, in *Liquids, Freezing and Glass Transition*, edited by J. P. Hansen, D. Levesque, and J. Zinn-Justin (North-Holland, Amsterdam, 1991), Chap. 10.

[2] A. Liu and S. R. Nagel, Nature (London) **396**, 21 (1998).

[3] M. Dzugutov, Nature (London) **381**, 137 (1996).

[4] Y. Rosenfeld, J. Phys. Condens. Matter **11**, 5415 (1999).

[5] M. Dzugutov, J. Phys. Condens. Matter **11**, A253 (1999).

[6] A. Samanta, Sk. Musharaf. Ali, and S. K. Ghosh, Phys. Rev. Lett. **87**, 245901 (2001).

[7] W. P. Krekelberg, M. J. Pond, G. Goel, V. K. Shen, J. R. Errington, and T. M. Truskett, Phys. Rev. E **80**, 061205 (2009).

[8] J. J. Hoyt, M. Asta, and B. Sadigh, Phys. Rev. Lett. **85**, 594 (2000).

[9] G. X. Li, C. S. Liu, and Z. G. Zhu, Phys. Rev. B **71**, 094209 (2005).

[10] J. C. Crocker and D. G. Grier, J. Colloid Interface Sci. **179**, 298 (1996).

[11] B. P. Binks and T. Horozov, *Colloidal Particles at Liquid Interfaces* (Cambridge University Press, Cambridge, England, 2006).

[12] P. Pieranski, Phys. Rev. Lett. **45**, 569 (1980).

[13] N. D. Denkov, O. D. Velev, P. A. Kralchevsky, I. B. Ivanov, H. Yoshimura, and K. Nagayama, Nature (London) **361**, 26 (1993).

[14] T. O. E. Skinner, D. G. A. L Aarts, and R. P. A. Dullens, Phys. Rev. Lett. **105**, 168301 (2010).

[15] J. R. Savage, D. W. Blair, A. J. Levine, R. A. Guyer, and A. D. Dinsmore, Science **314**, 795 (2006).

[16] Z. Zheng, F. Wang, and Y. Han, Phys. Rev. Lett. **107**, 065702 (2011).

[17] Z. Zhang, N. Xu, D. T. N. Chen, P. Yunker, A. M. Alsayed, K. B. Aptowicz, P. Habdas, A. J. Liu, S. R. Nagel, and A. G. Yodh, Nature (London) **459**, 230 (2009).

[18] F. Ghezzi and J. C. Earnshaw, J. Phys. Condens. Matter **9**, L517 (1997).

[19] J. Ruiz-Garcia, R. Gamez-Corrales, and B. I. Ivlev, Phys. Rev. E **58**, 660 (1998).

[20] W. Chen, S. S. Tan, T. K. Ng, W. T. Ford, and P. Tong, Phys. Rev. Lett. **95**, 218301 (2005).

[21] W. Chen, S. S. Tan, Z. S. Huang, T. K. Ng, W. T. Ford, and P. Tong, Phys. Rev. E **74**, 021406 (2006).

[22] M. Sickert, F. Rondelez, and H. A. Stone, Europhys. Lett. **79**, 66 005 (2007).

[23] V. Prasad, S. A. Koehler, and E. R. Weeks, Phys. Rev. Lett. **97**, 176001 (2006).

[24] Y. Peng, W. Chen, T. M. Fischer, D. A. Weitz, and P. Tong, J. Fluid Mech. **618**, 243 (2009).

[25] M. H. Lee, S. P. Cardinali, D. H. Reich, K. J. Stebeb, and R. L. Leheny, Soft Matter **7**, 7635 (2011).

[26] J. L. Bretonnet, J. Chem. Phys. **117**, 9370 (2002).

[27] F. Ebert, P. Dillmann, G. Maret, and P. Keim, Rev. Sci. Instrum. **80**, 083902 (2009).

[28] See Supplemental Material http://link.aps.org/supplemental/10.1103/PhysRevLett.110.078302 for more details about the apparatus and experimental methods.

[29] A. Baranyai and D. J. Evans, Phys. Rev. A **40**, 3817 (1989).

[30] W. Chen and P. Tong, Europhys. Lett. **84**, 28 003 (2008).

[31] N. Xu, D. Frenkel, and A. J. Liu, Phys. Rev. Lett. **106**, 245502 (2011).

[32] V. N. Michailidou, G. Petekidis, J. W. Swan, and J. F. Brady, Phys. Rev. Lett. **102**, 068302 (2009).